Highly Dynamic Ligand Binding and Light Absorption Coefficient of Cesium Lead Bromide Perovskite Nanocrystals

Jonathan De Roo,[†,‡,¶,§] Maria Ibáñez,[§,‖] Pieter Geiregat,[‡,⊥] Georgian Nedelcu,[§] Willem Walravens,[‡,⊥] Jorick Maes,[‡,⊥] José C. Martins,[¶] Isabel Van Driessche,[†] Maksym V. Kovalenko,[*,§,‖] and Zeger Hens[*,‡,⊥]

Sol-gel Center for Research on Inorganic Powders and Thin films Synthesis (SCRiPTS), Ghent University, Ghent, Belgium, Physics and Chemistry of Nanostructures group (PCN), Ghent University, Ghent, Belgium, NMR and Structure Analysis Unit, Ghent University, Ghent, Belgium, Laboratory of Inorganic Chemistry, ETH Zürich, Zürich, Switzerland, Laboratory for Thin Films and Photovoltaics, Empa – Swiss Federal Laboratories for Materials Science and Technology, Dübendorf, Switzerland, and Center for Nano and Biophotonics, Ghent University, Ghent, Belgium

E-mail: mvkovalenko@ethz.ch; zeger.hens@ugent.be

Abstract

Lead halide perovskite materials have attracted significant attention in the context of photovoltaics and other optoelectronic applications and recently, research efforts have been directed

[*]To whom correspondence should be addressed
[†]SCRiPTS, Ghent University
[‡]PCN, Ghent University
[¶]NMRSTR, Ghent University
[§]ETH Zürich
[‖]Empa, Zürich
[⊥]NB-Photonics, Ghent University

to nanostructured lead halide perovskites. Collodial nanocrystals (NCs) of cesium lead halides ($CsPbX_3$, X = Cl, Br, I) exhibit bright photoluminescence, with emission tunable over the entire visible spectral region. However, previous studies on $CsPbX_3$ NCs did not address key aspects of their chemistry and photophysics such as surface chemistry and quantitative light absorption. Here we elaborate on the synthesis of $CsPbBr_3$ NCs and their surface chemistry. In addition, the intrinsic absorption coefficient was determined experimentally by combining elemental analysis with accurate optical absorption measurements. ^{1}H solution nuclear magnetic resonance spectroscopy was used to characterize sample purity, to elucidate the surface chemistry and to evaluate the influence of purification methods on the surface composition. We find that ligand binding to the NC surface is highly dynamic, and therefore, ligands are easily lost during the isolation and purification procedures. However, when a small amount of both oleic acid and oleylamine are added, the NCs can be purified, maintaining optical, colloidal and material integrity. In addition, we find that a high amine content in the ligand shell increases the quantum yield due to the improved binding of the carboxylic acid.

Since the discovery of hybrid organic-inorganic halide perovskite materials as highly efficient light absorbers in photovoltaic devices,[1–5] research activities have soared and applications are found in X-ray detectors,[6] photodetectors,[7] LED's[8] and lasing.[9,10] Recently, efforts were directed to the synthesis of these perovskites as nanocrystals (NCs). Either hybrid organic-inorganic (*i.e.*, RNH_3PbX_3[11–17]) or fully inorganic (*e.g.*, $CsPbX_3$[18–21]) colloidal nanocrystals were synthesized and they show great promise regarding photoluminescence (PL) quantum yield and color tunability. However, their surface chemistry remains unexplored, leading to difficulties in the development of effective isolation and purification procedures whilst maintaining outstanding PL properties. Compared to the classical chalcogenide quantum dots, $CsPbX_3$ are more ionic in nature and the interactions with capping ligands is also more ionic and labile. Consequently, when polar solvents are added to isolate the nanocrystals, the $CsPbX_3$ NCs often lose their bright PL, colloidal stability and sometimes even structural integrity. These observations call for an exhaustive investigation and insight in the surface chemistry of $CsPbX_3$ NCs.

Over the last 5 years, it has been shown that the binding of ligands to nanocrystals can be conveniently described by the Covalent Bond Classification (CBC), as developed by Green[22,23] to classify metal–ligand interactions and the ensuing complexes. Here, ligands are defined as L–, X– or Z–type, depending on the number of electrons that the neutral ligand contributes to the metal–ligand bond (2, 1 or 0, respectively). Various (cation–rich) metal sulfide and selenide nanocrystals, including for example CdSe, CdTe, PbS and PbSe, proved to be coordinated by X–type ligands such as carboxylates or phosphonates that bind to excess surface cations with a binding motif abbreviated as $NC(MX_n)$, where NC refers to the charge neutral, stoichiometric nanocrystal and M equals a metal $n+$ cation (Figure 1).[24] A more involved binding motif was demonstrated in the case of metal oxide nanocrystals such as HfO_2 or ZrO_2. These stoichiometric NCs proved to be passivated by dissociated carboxylic acids, which brings 2 different X–type ligands on the surface — the carboxylate and the proton — in a binding motif abbriviated as $NC(X)_2$.[25,26] L–type ligands are Lewis bases and Z–type ligands are Lewis acids that in the case of binary nanocrystals will coordinate to acidic (surface cations) or basic (surface anions) surface sites, respectively. Such

binding motifs can be concisely written as NC(L) and NC(Z) (Figure 1). Note that CdSe(CdX_2) can be considered as both NC(MX_2) or NC(Z) as ligand exchange reactions might invoke either only the X–type ligand exchange or the displacement of the entire MX_2 moiety. Such ligand exchange reactions can be concisely written with the proposed binding motif nomenclature (Table 1).

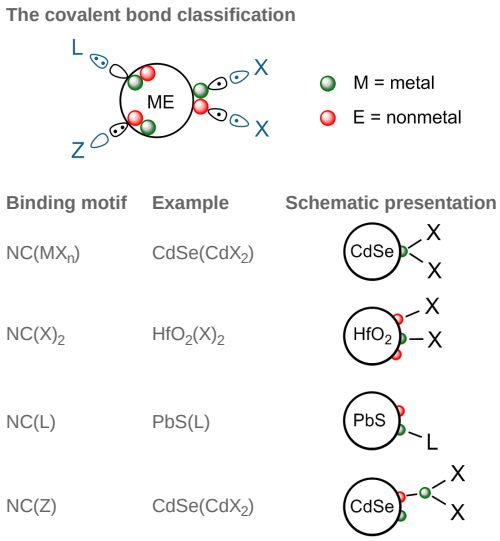

Figure 1: Schematic representation of the most important ligand classes within the covalent bond classification scheme. L–type ligands are Lewis bases, donating 2 electrons to the NC–Ligand bond. Z–type ligands are Lewis acids, offering an empty orbital while X–type ligands offer 1 electron. Schematic representations reflect the observable chemical reactivity of the ligand shell, not the atomistic details of the surface (basically unknown). For instance, NC(MX_n) and NC(Z) can correspond to the very same structure, such as CdSe(CdX_2).

One of the most powerful tools to study the organic–inorganic interface of the NC ligand shell and unravel binding motifs is Nuclear Magnetic Resonance (NMR) spectroscopy. One-dimensional, solution ^{1}H and ^{31}P NMR are readily accessible and were shown to aid considerably in the elucidation of NC–ligand interactions,[27–32] and the effect of purification procedures.[33,34] ^{1}H NMR in particular has the possibility to go beyond the structure analysis of organic compounds in solution and can effectively probe the dynamics of ligand–NC binding. Two-dimensional Diffusion Ordered Spectroscopy (DOSY) enables the molecular diffusion coefficient to be determined. This diffusion coefficient decreases (*i.e.*, slower translation) when a ligand is bound to a NC.[32] However, in cases where the ligand exchanges fast between a bound and a free state, only an av-

Table 1: Overview of different exchange reactions, their concise notation and examples. $NC(MX_2)$ can be involved in either an X'–for–X exchange or an L–type promoted Z–type displacement.

Exchange reaction	**Example**
$NC(X)_2 + 2L \rightleftharpoons NC(L) + \left[(LX)^+(X)^-\right]$	Displacement of dissociated carboxylic acid by amines from HfO_2 NCs, driven by ion-pair formation[25]
$NC(MX_2) + 2HX' \rightleftharpoons NC(MX'_2) + 2HX$	Exchange of carboxylate for phosphonate ligands on CdSe NCs[46]
$NC(MX_2) + (n+1)L \rightleftharpoons NC(L) + MX_2L_n$	Displacement of Cd carboxylate by amines from CdSe NCs driven by complex formation[27]

erage diffusion coefficient is measured. Therefore, it is difficult to assess ligand binding when the fraction of free ligand is much larger than the bound fraction. In that case a NOESY (Nuclear Overhauser Effect Spectroscopy) NMR experiment can ascertain ligand binding since the NOE effect is strongly dominated by the bound fraction.[35]

Here we focus on inorganic $CsPbBr_3$ NCs, synthesized by an approach slightly modified from the protocol reported by Protesescu *et al.*[18] and gain more insight in the underlying chemical reactions and surface chemistry. We performed ICP–MS (Inductively Coupled Plasma – Mass Spectrometry) and light absorption measurements and thus determined the intrinsic absorption coefficient. We use it to accurately estimate the $CsPbBr_3$ isolation/purification yield and the NC concentration. *Via* solution ^{1}H NMR, we show that difficulties with the purification arise from the dynamic nature of the NC–ligand bonding and demonstrate that this problem can be tackled by manipulating the bonding equilibrium with an excess of free ligands. Both carboxylic acids and long chain amines were found necessary to stabilize the surface during purification steps, however for optimal PL quantum yield, amines proved key. Similar to what has been found with metal oxide NCs, our findings indicate $CsPbBr_3$ NCs are terminated by pairs of X–type ligands — either oleylammonium bromide or oleylammonium carboxylate — yielding a $NC(X)_2$ binding motif. This work sheds thus more light on the surface chemistry of $CsPbBr_3$ NCs and opens the way for

further surface modifications, required for the optoelectronic applications of these NCs.

Results and discussion

Synthesis

$CsPbBr_3$ NCs are prepared by the injection of cesium oleate in an octadecene solution containing $PbBr_2$, oleic acid and oleylamine. Note that the reagents were used as received, without additional purification or drying. Immediately after injection of cesium oleate at 180 °C, the NCs precipitate from the solution (see Figure 2A) and are collected by centrifugation and redissolution in hexane. More illustrative photographs concerning the synthesis process can be found in the supporting information (Figure S1). A small excess of oleic acid and oleylamine is added and the NCs are precipitated with acetone and redispersed in hexane (see Methods section for experimental details). The NCs have an average cube edge length of 8.4 nm according to transmission electron microscopy (TEM, Figure 2B) and have a cubic crystal structure as attested by the XRD (x–ray diffraction) diffractogram, see Figure 2C. The absorption spectrum (Figure 2D) shows the first excitonic peak at 498 nm and a PL centered at 508 nm with a FWHM (full width at half maximum) of 19 nm. The PL quantum yield of a purified sample was determined at 83%. However, as we shall see further, the PL quantum yield is strongly dependent on the properties of the NC surface and therefore on the manipulation of NC colloids.

To gain more insight in the complex reaction mixture and therefore the nature of possible ligands, it is helpful to consider the underlying reaction mechanism. We can formally write the perovskite formation reaction as:

$$2\,Cs(OOCR) + 3\,PbBr_2 \longrightarrow 2\,CsPbBr_3 + Pb(OOCR)_2 \qquad OOCR = \text{oleate} \qquad (1)$$

Lead oleate is an obvious by–product of the synthesis and full yield in lead can thus never be achieved with these reagents. However, this reaction is performed with a lead bromide excess and

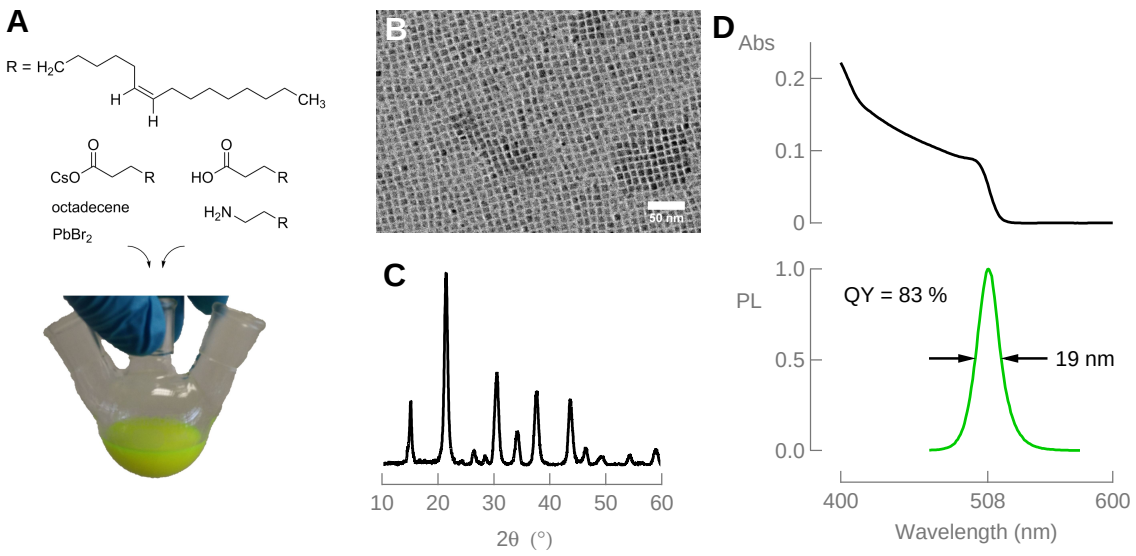

Figure 2: (A) Schematic overview of the reagents and outcome of a $CsPbBr_3$ NC synthesis. (B) TEM image (C) XRD diffractogram, showing the cubic perovskite phase (D) UV–VIS and normalized PL of a standard $CsPbBr_3$ synthesis, purified with the standard protocol as described in the Methods section. For PL, the excitation wavelength was 460 nm and 5 vol% oleylamine was added to the suspension prior to dilution for quantum yield determination.

cesium oleate is the limiting reagent. The recognition that lead oleate is formed is important since it is known to act as a ligand towards NC surfaces, such as in the case of PbS NCs.[27]

Equation 1 describes the overall reaction, but in reality neat octadecene does not dissolve $PbBr_2$. Moreover, neither the addition of 8 equivalents of oleylamine nor that of oleic acid was sufficient to dissolve $PbBr_2$, only the addition of both succeeded in complete dissolution. This suggests an early stage anion exchange between lead bromide and oleic acid, aided by the formation of oleylammonium bromide (oleylamine binds HBr).

$$PbBr_2 + x\,HOOCR + x\,RNH_2 \longrightarrow PbBr_{(2-x)}(OOCR)_x + x\,RNH_3Br \qquad x = 1 \text{ or } 2 \qquad (2)$$

Therefore, at the end of the reaction, the synthesis mixture probably comprises — apart from NCs — lead oleate, oleylammonium bromide, oleic acid and oleylamine, which are all potent surface binding species.

Indirect confirmation that Equation 2 applies – and an interesting synthesis variation – is found

when octadecene and oleic acid are replaced by oleylamine, thus having pure oleylamine as solvent. Heated to 120 °C, $PbBr_2$ dissolves in oleylamine and the solution is slightly yellow–green, probably due to the coordination of amines to the metal center. Nonetheless, addition of oleic acid at this stage, results in a colorless solution, thus experimentally confirming the interaction between oleic acid and $PbBr_2$. If, instead of oleic acid, cesium oleate is injected in the solution at 180 °C, $CsPbBr_3$ NCs are formed and do not immediately precipitate, in contrast to the standard synthesis in octadecene. Unfortunately, the particles degrade during the cool down to room temperature, probably due to a reaction with the excess of amine. This can be prevented by quenching the reaction mixture with an excess of toluene. Such NCs are very polydisperse but still have a PL centered around 510 nm with a FWHM of 21 nm (TEM, UV–VIS and PL in Figure S2).

The intrinsic absorption coefficient

A convenient feature of colored materials is their concentration dependent light absorption as described by the law of Bouguer–Lambert–Beer, which makes for a swift way of determining the NC volume fraction and concentration in a NC dispersion. Here, the intrinsic absorption coefficient μ_i is a most convenient quantity as it was found to be independent of the NC size for various quasi–spherical semiconductor NCs at photon energies well above their band gap.[36] By definition, μ_i is related to the absorbance A of a NC dispersion, the volume fraction f of the NC material, defined as the ratio between the NC volume and the dispersion volume, and the optical pathlength L:

$$\mu_i = \frac{\ln 10 A}{fL} \tag{3}$$

Hence, the combination of μ_i and an absorbance measurement of a given sample allows for the determination of the amount of NC material (the total volume of $CsPbBr_3$) and the NC concentration (if the average volume of a NC is known).

Here, we obtained μ_i by combining elemental analysis and UV–Vis absorption spectroscopy on the same sample. For elemental analysis, three samples were taken from the same $CsPbBr_3$

NC reaction. After careful purification, each sample was dried and digested in a known amount of HNO_3 and analyzed for its Pb and Cs content using ICP–MS. The samples feature a Pb:Cs ratio of 1.00 (see Supporting Information Table S1), a result indicating that the sample preparation indeed effectively separated NCs from residual reagents or the lead oleate by–product. Using the Pb content to determine the $CsPbBr_3$ volume fraction in the original samples, a μ_i spectrum for each aliquot could be calculated according to Equation 3. The corresponding average μ_i spectrum is shown in Figure 3A, where the gray area represents the error on the analysis and the inset shows the variation on $\mu_{i,335}$, *i.e.*, the intrinsic absorption coefficient at 335 nm, of the different samples and the thus obtained average value is $2.0 \pm 0.1\, 10^5\, \mathrm{cm}^{-1}$.

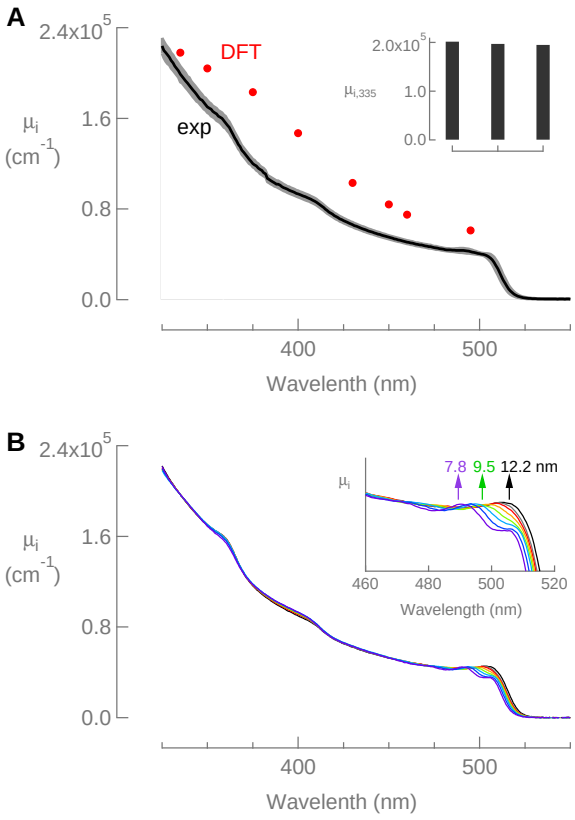

Figure 3: (A) The experimental spectrum of the intrinsic absorption coefficient (determined by a combination of UV–VIS and ICP–MS) and the effective–medium–theory predictions based on a complex dielectric function determined by density functional theory (DFT).[37] The gray area represents the error on the experimental μ_i spectrum and the inset shows the different values at 335 nm for the different ICP/UV–VIS samples. (B) UV–VIS spectra of different sized $CsPbBr_3$ NCs, obtained by size selective precipitation, details are provided in methods section and the supporting information.

The intrinsic absorption coefficient of a dispersed colloid depends on the complex dielectric function $\varepsilon_d = \varepsilon_{d,r} + i\varepsilon_{d,i}$ of the NC, the refractive index of the (presumed optically transparent) solvent $n_s = \sqrt{\varepsilon_s}$ and the wavelength of light λ:

$$\mu_i = \frac{2\pi}{\lambda n_s} |f_{LF}|^2 \varepsilon_{d,i} \tag{4}$$

Here, f_{LF} denotes the so–called local field factor, which is the ratio between the electric field inside a NC and the incident electric field. For a spherical particle, it reads:

$$f_{LF} = \frac{3\varepsilon_s}{\varepsilon_d + 2\varepsilon_s} \tag{5}$$

Having the complex dielectric function of a material thus allows to predict an intrinsic absorption coefficient. On the other hand, experimental data on the intrinsic absorption coefficient could be used to validate the calculation of complex dielectric functions by first–principles. As an example, we used the bulk dielectric function of $CsPbBr_3$ obtained by a density functional theory study[37] to calculate a theoretical intrinsic absorption coefficient of cubic $CsPbBr_3$ NCs. As shown in Figure 3A, not all features of the experimental spectrum are closely followed by the predicted values, yet the order or magnitude is correct and especially at shorter wavelengths, the theoretical and experimental absorption coefficient seem to match.

Note that for a given NC shape and a given solvent, Equations 4 and 5 imply that μ_i will be independent of NC size when ε_d is size–independent. This situation is typically seen with semiconductor NCs at wavelengths considerably shorter than their band–gap transition. Figure 3B therefore shows absorption spectra of $CsPbBr_3$ dispersions containing NCs with different average diameters (see Supporting Information Figure S3), normalized at $\mu_{i,335} = 2.0\,10^5\,\mathrm{cm}^{-1}$. The spectra are obviously size-dependent around the band-gap transition and some size-variation remains at the features around 360 and 400 nm. On the other hand, they coincide surprisingly well in wavelength regions where the absorption is largely featureless, such as 325–345 nm, and 415–455 nm. The concomitant absorption coefficients can thus also be used for analysing the $CsPbBr_3$ volume

fraction in NC dispersions, irrespective of the NC size and a tabulated absorption coefficient spectrum is therefore added to the Supporting Information. For one thing, having a size–independent absorption coefficient leads to an analytical expression of the molar extinction coefficient ε_{335} — linking absorbance at 335 nm to NC concentration — of $CsPbBr_3$NCs:

$$\varepsilon_{335} = \frac{N_A V_{NC}}{\ln 10} \mu_i \approx (0.052 \pm 0.002)\, d^3\, \mathrm{cm}^{-1}\, \mu\mathrm{M}^{-1} \tag{6}$$

Here, N_A is Avogadro's number, V_{NC} the nanocrystal volume and d is the cube edge in nanometer.

Importantly, even if ε_d is size–independent, intrinsic absorption coefficients of NCs will depend on the NC shape. Hence, shape differences may compromise the analysis of volume fractions in different NC samples using a single, size–independent absorption coefficient. Since $CsPbBr_3$ NCs typically feature a cubic shape, we therefore used the theoretical dielectric function of $CsPbBr_3$ to calculate μ_i for cubic and spherical NCs (Figure S4). The resulting absorption coefficients only differ by $\approx 10\%$, a result indicating that the experimentally determined absorption coefficients here on a sample of cubic $CsPbBr_3$ NCs can be used for analysing spherical NCs without introducing major errors. Importantly, a similar conclusion will also apply to, *e.g.*, $CsPbCl_3$ NCs, but not to $CsPbI_3$ or PbS NCs as the imaginary part of the dielectric function is so large for these materials that deviations between both values become unacceptable (up to 50 %, see calculations in SI and Figure S4).

Having $\mu_{i,335}$, we are now able to characterize the $CsPbBr_3$ NC synthesis in terms of chemical yield, where we find that the relatively monodisperse fraction as displayed in Figure 2 after isolation and purification represents a yield of only 15 %. However, a large fraction of the NCs was discarded in the isolation process. To increase the isolation yield of the synthesis, acetone can be added to the raw synthesis mixture, prior to the first centrifugation step and the precipitate is dispersed in 10 mL of hexane. This mixture was then again purified with acetone and small amounts of oleylamine and oleic acid and the final yield was 82% but the particles are more polydisperse (see TEM in Figure S5). Interestingly, the PL is still quite narrow (FWHM = 21 nm) but slightly

redshifted to 514 nm (Figure S5), consistent with the larger particle size in TEM.

Surface of as–synthesized NCs

It is common practice in NC syntheses to purify NCs by multiple precipitation/redispersion steps using polar solvents such as ethanol, methanol, isopropanol, acetone, acetonitrile or ethyl acetate. However, when these solvents are added in excess, the $CsPbBr_3$ NCs loose their PL, colloidal stability and often even structural integrity. In this respect, a slightly higher robustness was noted when using non–dried solvents during synthesis. Small amounts of acetone or acetonitrile can be added, precipitating part of the $CsPbBr_3$ NCs. Another part of the NCs is apparently lost as the supernatant after centrifugation is strongly colored. The precipitate is redispersed in hexane, resulting in a green suspension. Unfortunately, in the ^{1}H NMR spectrum of such a 'purified' suspension, we observe the characteristic resonances of a terminal alkene — presumable octadecene (ODE) — at 4.94 and 5.8 ppm (Figure 4A) indicating that this sample is insufficiently purified (all reference spectra of oleic acid, oleylamine and ODE are presented in Figure S6). Comparing with the reference spectrum of oleic acid, we also recognize the characteristic resonances **1** and **2** of oleic acid in the sample. These resonances have fine structure and appear at exactly the same chemical shift as the reference, as opposed to the typical behaviour of bound ligands, which feature broadened and slightly shifted resonances. Resonances **3**, **4** and **6** of oleic acid show overlap with those of oleylamine and octadecene and are therefore of little use. The very broad resonances α and β are ascribed to the NH_3^+ and α–CH_2 of oleylammonium respectively, in compliance with earlier reports,[26] and a more detailed argumentation is provided in the supporting info, see Figure S7. The presence of (protonated) oleylamine is also confirmed by analysis of resonance **5** at 5.33 ppm, which corresponds to the alkene resonance of either oleylamine, oleic acid or both. The total concentration of oleyl species (determined from resonance **5**) is 8.3 mM while the concentration of oleic acid (determined from resonance **1**) is 5.1 mM. The difference (3.2 mM) is ascribed to the presence of (protonated) oleylamine. Although peak broadening typically indicates bound ligands, it is uncommon for the protons, closest to the surface, to be detected.[25] This conundrum will be

addressed further on.

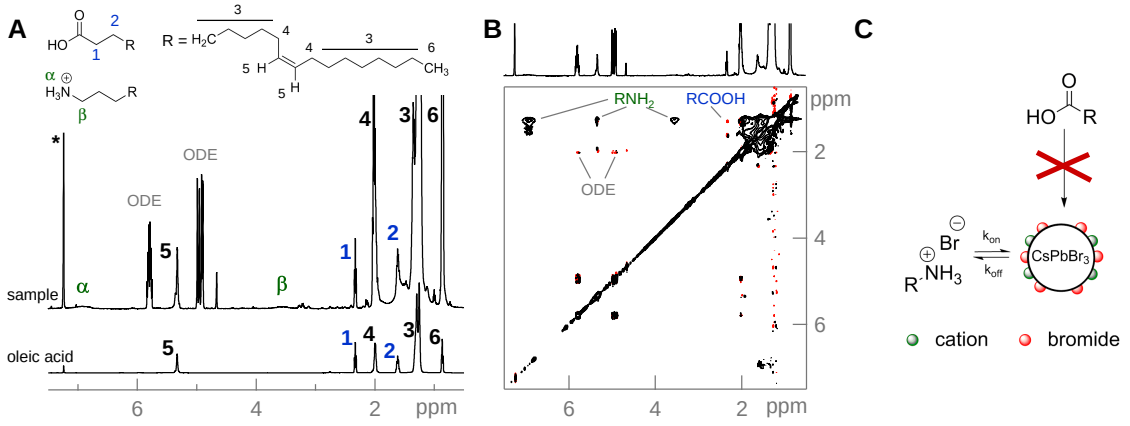

Figure 4: (A) ^{1}H NMR spectrum 8.4 nm $CsPbBr_3$ NCs purified with acetone and filtered. Concentration of QDs: 2.2 μM. The reference spectrum for **oleic acid** is displayed and impurities of octadecene (ODE) are also indicated. (B) NOESY spectrum of the sample purified with acetone in $CDCl_3$. (C) Schematic representation of the dynamic surface stabilization by oleylammonium bromide. Oleic acid is not part of the ligand shell.

The NOESY spectrum (Figure 4B) confirms that octadecene and oleic acid are not bound to the $CsPbBr_3$ NCs as they feature positive (red) cross peaks, which is conclusive proof for lack of interaction with the surface.[38] The observation that oleic acid does not bind is in accordance with an earlier report on the stoichiometric nature of the $CsPbBr_3$ NCs.[18] Indeed, to bind as a negative X–type ligand, the negative charge of the oleate would require compensation by a cationic excess on the surface, which is not present. In order to bind in a $NC(X)_2$ binding motif — in a dissociative mode with both proton and oleate as ligand[25] — the NC's anion should have a high affinity towards protons, which is not the case for bromide (HBr is significantly more acidic than oleic acid). In constrast, the negative (black) cross peaks between the resonances of oleylamine corroborate the interaction of oleylamine with the surface. In light of the previously described chemical equations, ligand possibilities and protonated state of oleylamine, we infer that oleylammonium bromide is the acting ligand in this sample. This is a pair of X–type ligands, binding with the oleylammonium cation to surface bromide — presumably through a hydrogen bridge — and with the bromide anion to the surface cesium or lead ions, see Figure S8. It is no surprise that the highly ionic $CsPbBr_3$ NCs prefer ionic ligands, compared to ligands that bind with a highly covalent character such as

lead oleate.

To gain more insight in the dynamics of stabilization, the diffusion coefficient D of a molecule is a helpful parameter as the diffusion coefficient of a bound ligand is equal to the diffusion coefficient of the total object (NC plus ligand shell). The diffusion coefficient can be obtained from Diffusion Ordered NMR Spectroscopy (DOSY) and can be related to the size of the molecule *via* the Stokes–Einstein equation with f the friction coefficient, k_B the Boltzmann constant and T the absolute temperature:

$$D = \frac{k_B T}{f} \tag{7}$$

For spherical particles, the friction coefficient is $f = 6\pi\eta r_s$ (η the solvent's viscosity, r_s the solvodynamic radius of the object/molecule) and this expression was already repeatedly used to calculate the solvodynamic radius of NCs from DOSY data.[26,32,39–41] For non–spherical NCs, the friction coefficient needs adjusting[42,43] and the general expression is $f = 6\pi\eta C$ with C the so–called capacity of the object.[44] Although there is no previous account of DOSY NMR on cubic NCs, Hubbard[44] and Douglas[45] calculated the capacity of arbitrary shaped objects. For a cube, the capacity proved $C = 0.66d$ with d the cube edge length and we will use this relation throughout this paper.

From DOSY measurements we obtained the diffusion coefficient of oleylammonium bromide in the NC suspension, $D = 166 \pm 18$ μm^2/s, significantly smaller than the diffusion coefficient in the absence of NCs ($D = 361$ μm^2/s). The decrease in D (slower diffusion) confirms the interaction of oleylammonium bromide with the NC surface, as already indicated by the NOESY analysis. However, 166 μm^2/s corresponds to a cube edge length of 3.7 nm, clearly smaller than expected, as the NCs measure 8.4 nm in TEM. This observation implies that the oleylammonium bromide is not tightly bound to the NC surface but exchanges fast between its bound and free state[38] and therefore, an average diffusion coefficient is measured. This highly dynamic stabilization mechanism with oleylammonium bromide may well explain the ease of anion exchange reactions with these nanocrystals.[19,21] Particularly the observation of an inter–NC anion exchange when two parent NCs (*e.g.*, $CsPbBr_3$ and $CsPbCl_3$) are mixed in solution, advocates for the dynamic interaction

of oleylammonium halides with the surface. Unfortunately, the dynamic stabilization is also the origin of purification difficulties, as the desorption of oleylammonium bromide in polar solvents will proceed swiftly.

If we assume that the NCs plus ligand shell would amount to an object of about 10 nm, the diffusion coefficient of the bound ligand fraction (D_2) can be estimated at 60 μm^2/s by Equation 7. Neglecting all other equilibria except for the ligand binding event, the diffussion coefficient of the free oleylammonium bromide ligand is $D_1 = 361$ μm^2/s. In case of fast exchange, the observed diffusion coefficient (D) is a weighed average of the fractions. Hence, the bound fraction can be calculated from the observed average diffusion coefficient and the diffusion coefficients of either fraction:

$$x = \frac{D_1 - D}{D_1 - D_2} \tag{8}$$

Using Equation 8, we thus estimate the bound fraction at 65%. This rather high fraction of bound ligands, yet in fast exchange with a pool of free ligands, explains why the resonances α and β — being close to the surface — are broadened yet still detectable in the ^{1}H NMR spectrum (Figure 4). After all, the line width is also an average between the free and bound state.

For the same sample, the ^{1}H NMR spectrum yields a total oleylammonium bromide concentration of 3.3 mM, which means 2.15 mM is in the bound state. Together with the NC concentration of 2.2 μM (calculated with the molar extinction coefficient for 8.4 nm NCs, *vide supra*), we calculate a ligand density of 2.3 ligands nm^{-2}. Considering the lattice parameter (0.587 nm) and the crystal structure, there is one cation/anion pair per 0.344 nm^2 of surface, resulting in a theoretical ligand density of 2.9 nm^{-2}. The close correspondence with the experimental value indicates almost complete passivation of the surface and indeed, the suspension is brightly green luminescent.

Oleylamine draws oleic acid into the ligand shell

The chemical shift of the α resonance in Figure 4 suggests that oleylamine is almost 100% in its protonated state. However, the acidic proton can be rapidly transfered to an unprotonated amine

and therefore, the α and β resonances sharpen and shift in the spectrum when 25 mM of unprotonated oleylamine is added to the NC dispersion (Figure 5A). In particular, we observe the averaged resonances at a chemical shift position between the original position and the position in the reference spectrum of oleylamine. Since the unprotonated amine is added in almost tenfold excess, the β resonance has a chemical shift, close to the reference chemical shift (Figure 5A). In addition, the diffusion coefficient increased to 681 ± 10 μm^2/s, again an average over all the populations but closest to the diffusion coefficient of pure oleylamine: 880 ± 10 μm^2/s (as expected because of the high excess). We conclude that oleylamine is primarily in the free, unprotonated state but is involved in several equilibria.

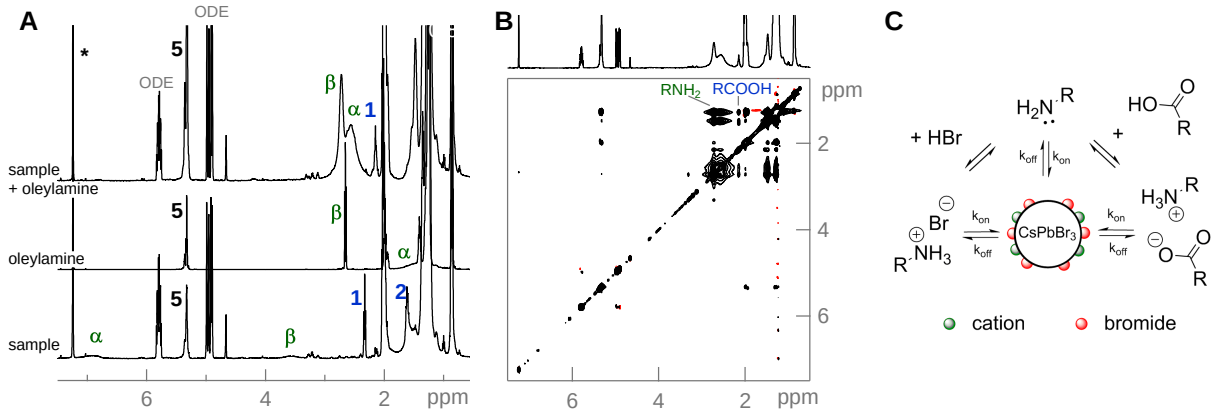

Figure 5: (A) ^{1}H NMR spectrum 8.4 nm $CsPbBr_3$ NCs purified with acetone and filtered, before and after addition of 5 μL of oleylamine. Concentration of QDs: 2.2 μM. The octadecene (ODE) impurities are also indictated. (B) NOESY spectrum of the sample + oleylamine. (C) Schematic representation of the dynamic surface stabilization by oleylammonium bromide, oleylammonium oleate and oleylamine. In addition, the relevant acid/base equilibria are depicted.

Interestingly, the NOESY spectrum in Figure 5B still features negative (black) nOe cross peaks for oleylamine, indicating that at least a fraction is still interacting with the surface. As it happens, oleylamine has many possibilities to do so, see Figure 5C. First, oleylamine is involved in the acid/base equilibrium with hydrogen bromide, and binds to the surface as oleylammonium bromide ($NC(X)_2$). Second, oleylamine can deprotonate oleic acid and form oleylammonium oleate. Indeed, resonance **1** of oleic acid has shifted to lower ppm values, consistent with deprotonation. In addition, the cross peaks of oleic acid in the NOESY spectrum have switched sign and are now

negative. Therefore, we infer that oleate is binding to the NC surface as an ion pair with oleylammonium. This is again an example of a pair of X–type ligands, coordinating to a stoichiometric surface; $NC(X)_2$. Once more, this surface ligation is highly dynamic because we observe an average diffusion coefficient of $D_{oleate} = 370 \pm 22$ $\mu m^2/s$. Although lower than the reference value for a mixture of oleic acid and oleylamine (575 $\mu m^2/s$), this diffusion coefficient is far from the expected diffusion coefficient of a tightly bound ligand (60 $\mu m^2/s$). Since the original surface was already fully passivated (see previous section), the observation that the oleylammonium oleate is binding to the surface, implies a ligand exchange of the orginal oleylammonium bromide:

$$NC(X)_2 + (X')^+(X')^- \longrightarrow NC(X')_2 + (X)^+(X)^- \tag{9}$$

Here, $(X')^+(X')^-$ and $(X)^+(X)^-$ are short hand descriptions of oleylammonium bromide and oleylammonium oleate as ion pairs of two X–type moieties. Third and last, oleylamine could also bind in its unprotonated state, as an L–type ligand coordinating to the surface cations. Again, this involves a ligand exchange:

$$NC(X)_2 + L \longrightarrow NC(L) + (X)^+(X)^- \tag{10}$$

We conclude that the single set of oleylamine resonances encompasses a large variety of states that exchange rapidly among each other. The negative nOe (Figure 5B) and lower diffusion coefficient (compared to pure oleylamine) indicate that at least one of these states is interacting with the surface. It is however impossible to disentangle the individual contributions.

Tightly bound oleylammonium oleate by large amine excess

To investigate the role of oleylamine in more detail, we added a relatively large amount (10 vol%) to an unpurified $CsPbBr_3$ NC suspension and only a small amount of acetone (50 vol%). This process precipitated part of the NCs and the precipitate could be redispersed in toluene after centrifugation. In Figure 6A the ^1H NMR spectrum in deuterated toluene is displayed. Again, oc-

tadecene resonances are present, in addition to the alkene resonance and the distinct resonance β of oleylamine. Focusing on the alkene resonance around 5.5 ppm, we observe a broad contribution shifted to slighty higher ppm values (5.65 ppm, indicated with an arrow). The NOESY spectrum (6B) reveals broad negative cross peaks for this broadened resonance, confirming its bound nature. Moreover, the sharp alkene resonance also features negative nOe cross peaks and there is a cross peak from the broad to the sharp alkene resonance, most probably due to chemical exchange (see inset Figure 6B). Such observations were already explained in earlier work, the broad resonance was assigned to tightly bound ligands, in slow exchange with weakly bound ligands, featuring sharp resonances.[24,27,29] Indeed, in the DOSY experiment we observed a slowly diffusing component with $D = 59 \pm 9$ μm^2/s. This diffusion coefficient corresponds to a cube edge length $d = 9.7 \pm 1.5$ nm, in agreement with NCs of 8.4 nm and an additional ligand shell, confirming the existence of a tightly bound ligand fraction. Despite this encouraging conclusion, the NCs are only stable for a limited amount of time and a fraction precipitates after 24 hours. However, the addition of a few microliters of trifluoroacetic acid brings the NCs back in suspension (brightly luminescing), again emphasizing the importance of acid–base equilibria in the NC stabilization, and pointing to the complexity of the involved surface reactions.

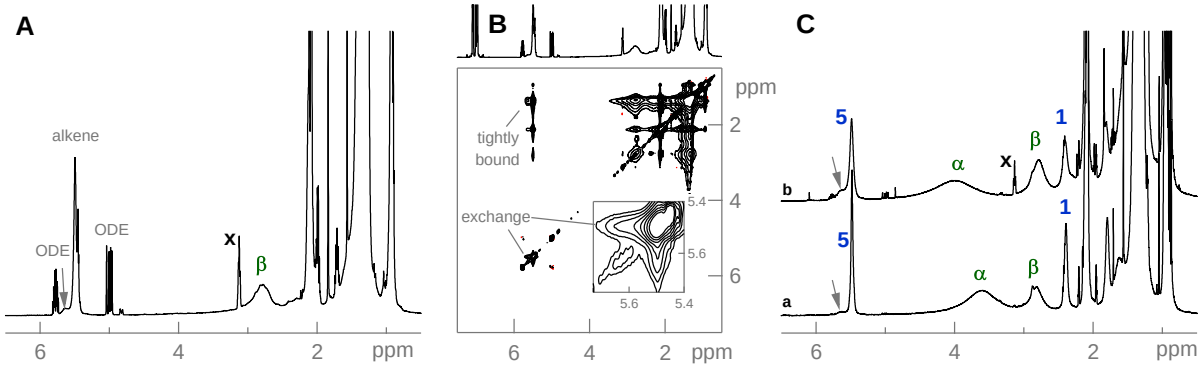

Figure 6: A. ^{1}H NMR spectrum of $CsPbBr_3$ NCs purified with 10 vol% oleylamine and acetone. The resonance denoted with x is an unknown impurity, presumbably the amide of oleic acid and oleylamine judging from its chemical shift. B. 2D NOESY spectrum of the sample in A. C. ^{1}H NMR spectrum of $CsPbBr_3$ NCs purified with 5 vol% oleic acid, 5 vol% oleylamine and acetone, three times (a) or 5 vol% oleic acid, 10 vol% of oleylamine and acetone, two times (b).

Although examples exist in literature of strongly bound amine ligands,[29,42] we cannot exclude

the tightly bound fraction to be composed of oleic acid since it will also contribute to the alkene resonance. In addition, the characteristic resonances of oleic acid (**1** and **2**) are not visible in the spectrum (Figure 6A), possibly because oleic acid is strongly bound to such large NCs, leading to excessive broadening of resonances close to the surface.[25] Therefore we decided to synthesize the $CsPbBr_3$ NCs with dodecylamine instead of oleylamine. We purified the sample 3 times by adding both dodecylamine and oleic acid before precipitation with acetone. This allowed us to quantitatively precipitate the NCs (colorless supernatant) and redisperse the NCs with excellent colloidal stability and bright luminescense. Firstly, the ^{1}H NMR spectrum does not feature any octadecene resonances (Figure 6C, sample **a**), the NCs are thus effectively purified. Secondly, although now both characteristic resonances of dodecylamine and oleic acid are recognized in the spectrum, only oleic acid contributes to the alkene resonance and therefore we conclude that the tightly bound fraction (indicated with an arrow) belongs to oleic acid. Since we previously concluded that oleic acid cannot bind by itself but only as an ion pair with amine, the actual tightly bound ligand will be alkylammonium oleate. In sample **b**, the ratio of dodecylamine to oleic acid during purification was increased and the appearance of the strongly broadened reasonance (the tightly bound fraction) is more pronounced (see Figure 6C, sample **b**, indicated by arrow), confirming the influence of the amine on the extent of the tightly bound fraction.

Implications on purification, quantum yield and applications

As–synthesized, the $CsPbBr_3$ NCs are stabilized with oleylammonium bromide, which is however in fast exchange between a free and bound state. Although the ligand density was found sufficiently high to fully passivate the surface in apolar media, the NCs lose colloidal and structural integrity and PL when polar solvents are added in excess, presumably due to rapid desorption of the ligand. Having established the surface as highly dynamic and the common purification methods as inadequate, we sought an improved protocol. When there is an excess of amine, also oleic acid can bind to the $CsPbBr_3$ NCs as an ion pair with oleylamine or dodecylamine. Addition of this ligand combination, prior to precipitation with acetone, proves essential to allow for multiple precipita-

tion and redispersion steps while maintaining colloidal stability and PL. Proceeding in this manner, octadecene contamination can be removed by three washing cycles. Caution is however needed, as a too high amount of surfactants causes decomposition of the NCs, *i.e.*, loss of color and formation of a white precipitate. A purified dispersion featured a quantum yield of 40 % but the addition of 5 vol% oleylamine to the disperison caused the quantum yield to increase to 83 %, probably due to a higher fraction of tightly bound oleate. Again there is a fine line between quantum yield optimization and NC decomposition due to excess of amine ($>$ 20 vol%). In addition, this tightly bound fraction does not prevent the complete dissolution of the NCs by large quantities of polar solvents, because the strongly bound fraction relies on an amine excess and controlled acid–base equilibria.

The behaviour of these $CsPbBr_3$ NCs is thus significantly different from classical oleate or phosphonate stabilized NCs (*e.g.*, CdSe, PbS, ...) where purified dispersions often contain only a monolayer of tightly bound ligands.[24–27,32,33,46,47] In this respect, the $CsPbBr_3$ NCs, stabilized by a pair of X–type ligands ($NC(X)_2$), better resemble the CdTe–dodecylamine systems (NC(L))[35] where a rapid exchange between bound and free ligands has also been established. To keep the NCs in dispersion — and certainly to precipitate them without desintegration — an excess of surfactants is always needed. This, of course, limits the number of applications. A possible solution to overcome these problems, might be to devise multidentate or even polymeric ligands, containing both carboxylic acid and amine groups. Such ligands might be found to be tightly bound as a single monolayer and without excess in solution. This can render the perovskite NCs suitable for applications such as organic–inorganic composites but still, applications where charge transport is required, will be hampered. Next to colloidal stability and PL, also the structural integrity is compromised by polar solvents. This may render the transfer to polar solvents all but impossible (except with a extensive, organic capping layer) which appears as an inherent limitation of these nanocrystals.

Conclusion

We have analyzed the synthesis of $CsPbBr_3$ NCs, gained new insights in the mechanism and provided alternative reaction conditions. We experimentally determined the intrinsic absorption coefficient of $CsPbBr_3$ NCs and found the wavelengths of 335 and 450 nm to be suited to analyze the volume fraction of a $CsPbBr_3$ NC dispersion. In addition, we established that a difference in NC shape (cubic versus spherical) only minorly influences the intrinsic absorption coefficient in case of $CsPbBr_3$ and $CsPbCl_3$ NCs but introduces large errors in the case of $CsPbI_3$ or PbS NCs. *Via* ^{1}H solution NMR we established the surface as dynamically stabilized with either oleylammonium bromide or oleylammonium oleate and we showed the inadequacy of standard solvent/non–solvent procedures for purification. This prompted us to add small amounts of excess oleic acid and oleylamine before precipitation, thereby preserving the colloidal integrity and photoluminescence of the NCs. In addition, the presence of an amine excess in the solution after purification causes the occurence of a strongly bound fraction of oleic acid and results in high quantum yields. The insights obtained in this paper could thus help to bridge the gap between the synthesis of these fascinating materials and their actual applications.

Methods

Preparation of Cs–oleate: 0.407 g of Cs_2CO_3 (2.5 mmol, Aldrich, 99.9%) was loaded into a 50 mL 3-neck flask along with 20 mL octadecene (octadecene, Sigma-Aldrich, 90%) and 1.55 mL oleic acid (5 mmol, oleic acid, Sigma Aldrich, 90%), dried for 1h at 120 °C, and then heated under N_2 to 150 °C until all Cs_2CO_3 dissolved. Since Cs–oleate is insoluble in octadecene at room temperature, it has to be preheated before injection. Final concentration: 0.116 M.

$CsPbBr_3$ synthesis: The required reagents and quantities are listed in Table 2. No special care was taken to dry solvents or surfactants. Either syntheses based on 138 mg or 69 mg $PbBr_2$ were performed. For a synthesis with 138 mg $PbBr_2$, the amounts of cesium and surfactants are doubled except that 7.5 mL octadecene was used. $PbBr_2$ is weighed in the glovebox and

transferred to a 25 mL 3–neck flask together with octadecene. The cloudy suspension is heated to 120 °C under vacuum or nitrogen. Subsequently, oleic acid and oleylamine are injected under nitrogen atmosphere (also other long chain amines such as dodecylamine can be used in equal molar amounts). After the quick dissolution of $PbBr_2$, the synthesis mixture is heated to 180 °C and Cs–oleate is injected. After 5 seconds, the cloudy, yellow mixture was cooled with a water bath and upon cooling the color changed to bright green. Illustrative photographs are provided in the supporting information (Figure S1).

Table 2: Reagents of a typical synthesis

	quantity	mmol	ratio on Pb
$PbBr_2$	69 mg	0.19	1
Oleylamine	0.5 mL	1.52	8.1
Oleic acid	0.5 mL	1.58	8.4
Cs–oleate solution	0.4 mL	0.046	0.25
Octadecene	5 mL		

Synthesis in oleylamine as solvent: 69 mg $PbBr_2$ was dispersed in 6 mL of oleylamine and put under vacuum for 5 minutes, then the temperature was raised to 120 °C and lead bromide dissolved. The temperature was raised to 180 °C and 0.4 mL Cs–oleate solution was injected. 2 seconds later, 15 mL of toluene was injected. After cooling down, the particles can be precipitated with acetone. The unpurified mixture has only limited long term stability (less than 24 hours).

Purification (for a synthesis based on 69 mg $PbBr_2$): the crude solution is centrifuged for 3 minutes at 10,000 rpm and the colored supernatant is discarded. 300 μL of hexane is added (or more to improve yield but resulting in a more polydisperse ensemble of NCs) and the NCs are dispersed by shaking. Then the suspension is centrifuged (3 min, 10,000 rpm) to discard larger NCs and agglomerates. Another 300 μL of hexane is added to the supernatant, resulting in a colloidally stable, green dispersion of $CsPbBr_3$ NCs. However, the dispersion still contains ODE and other impurities. To obtain only NCs and ligands, add 25 μL of both oleic acid and oleylamine and 600 μL of acetone. After centrifugation (3 min, 4400 rpm), the colorless supernatant is discarded and

600 μL of hexane is added to redisperse the NCs. This procedure can be repeated several times without destroying the NCs or decreasing their PL. To have less organics in the last mixture one can go down to adding only 5 μL of both ligands. This was the purification used for the ICP measurements but such dispersions have poor long term stability (less than one week).

Size selection (for a synthesis based on 138 mg lead bromide): The crude synthesis mixture is centrifuged and the colored supernatant is discarded. 150 μL of hexane is added to disperse the precipitate and this suspension is centrifuged. The supernatant containing small particles is discarded and another 150 μL hexane is added, followed by centrifugation to discard larger NCs and agglomerates. 300 μL of hexane is added to the supernatent, resulting in a colloidally stable dispersion of $CsPbBr_3$ NCs that is more monodisperse as the very small and very big NCs are discarded. To this refined dispersion, 20 μL of both oleylamine and oleic acid are added to preserve the PL of the NCs during the next steps. Now, acetone is added droplet by droplet until the dispersion turns cloudy. By centrifugation, a first fraction of NCs with a mean diameter of 12.6 nm can be collected (Figure 3). This procedure can be repeated over 10 times, each time yielding a fraction of dots with a smaller average diameter than the previous fraction. After ten cycles the mean diameter is reduced to 7.6 nm (Figure 3). The size was confirmed with TEM and the mentioned sizes are based on an ensemble of 100 particles.

General characterizaton: UV-Vis absorption spectra were collected using a Jasco V670 spectrometer in transmission mode. Fluorolog iHR 320 Horiba Jobin Yvon spectrofluorimeter equipped with a PMT detector was used to acquire steady–state PL spectra from solutions and films. The quantum yield was determined referenced to the standard dye fluorescein. The quantum yields provided in this paper were calculated as the average the quantum yields at excitation wavelengths of 440 and 460 nm. Powder X-ray diffraction patterns (XRD) were collected with STOE STADI P powder diffractometer, operating in transmission mode. Germanium monochromator, Cu Kα1 irradiation and silicon strip detector Dectris Mythen were used. Transmission electron microscopy (TEM) images were recorded using JEOL JEM-2200FS microscope operated at 200 kV. Details on the ICP analysis are found in the supporting info, section: the experimental molar extinction

coefficient.

NMR characterization: Nuclear Magnetic Resonance (NMR) measurements were recorded on a Bruker Avance III HD Spectrometer operating at a ^{1}H frequency of 500.26 MHz and equipped with a BBFO-Z probe. The sample temperature was set to 298.2 K. One dimensional (1D) ^{1}H and 2D NOESY (Nuclear Overhauser Effect Spectroscopy) spectra were acquired using standard pulse sequences from the Bruker library. For the quantitative 1D ^{1}H measurements, 64k data points were sampled with the spectral width set to 20 ppm and a relaxation delay of 30 sec. NOESY mixing time was set to 300 ms and 4096 data points in the direct dimension for 512 data points in the indirect dimension were typically sampled, with the spectral width set to 10 ppm. Diffusion measurements (2D DOSY) were performed using a double stimulated echo sequence for convection compensation and with monopolar gradient pulses.[48] Smoothed rectangle gradient pulse shapes were used throughout. The gradient strength was varied linearly from 2-95 % of the probe's maximum value in 32 or 64 increments, with the gradient pulse duration and diffusion delay optimized to ensure a final attenuation of the signal in the final increment of less than 10 % relative to the first increment. For 2D processing, the spectra were zero filled until a 4096 - 2048 real data matrix. Before Fourier transformation, the 2D spectra were multiplied with a squared cosine bell function in both dimensions, the 1D spectra were multiplied with an exponential window function. Concentrations were obtained using the Digital ERETIC method, as provided in the standard software of Bruker. The diffusion coefficients were obtained by fitting the appropriate Stejskal-Tanner equation to the signal intensity decay.[49]

Acknowledgement

The authors thank Mathias Grotevent for additional TEM measurements. JDR thanks the FWO (Research Foundation Flanders) for financial support. The authors thank Laura Piveteau for interesting scientific discussions. We thank the NMR Research Facility of the Laboratory for Inorganic Chemistry of the ETH Zürich for use of the NMR equipment. MVK and ZH acknowledge support by the European Comission via the Marie-Sklodowska Curie action Phonsi (H2020-MSCA-ITN-

642656). ZH acknowledges the FWO-Vlaanderen (project G.0760.12), the Belgian Science Policy office (IAP 7.35, photonics@be) and Ghent University (GOA 01G01513) for funding. MI thanks AGAUR for her Beatriu de Pinos postdoctoral grant.

Supporting Information Available

Covalent Bond Classification concepts; Explanatory photographs; TEM, UV-VIS and PL characterization of NCs synthesized with different protocols than the standard procedure; experimental data and calculations on the ICP–MS measurents and intrinsic absorption coefficient; Theoretical calculations on the intrinsic absorption coefficient; Additional NMR spectra; a spreadsheet with the experimental μ_i values at every wavelength

This material is available free of charge via the Internet at `http://pubs.acs.org/`.

References

1. Chung, I.; Lee, B.; He, J. Q.; Chang, R. P. H.; Kanatzidis, M. G. All-Solid-State Dye-Sensitized Solar Cells with High Efficiency. *Nature* **2012**, *485*, 486–489.

2. Green, M. A.; Ho-Baillie, A.; Snaith, H. J. The Emergence of Perovskite Solar Cells. *Nat. Photonics* **2014**, *8*, 506–514.

3. Hao, F.; Stoumpos, C. C.; Cao, D. H.; Chang, R. P. H.; Kanatzidis, M. G. Lead-Free Solid-State Organic-Inorganic Halide Perovskite Solar Cells. *Nat. Photonics* **2014**, *8*, 489–494.

4. Miyata, A.; Mitioglu, A.; Plochocka, P.; Portugall, O.; Wang, J. T. W.; Stranks, S. D.; Snaith, H. J.; Nicholas, R. J. Direct Measurement of the Exciton Binding Energy and Effective Masses for Charge Carriers in Organic-Inorganic Tri-Halide Perovskites. *Nat. Phys.* **2015**, *11*, 582–587.

5. Burschka, J.; Pellet, N.; Moon, S. J.; Humphry-Baker, R.; Gao, P.; Nazeeruddin, M. K.;

Gratzel, M. Sequential Deposition as a Route to High-Performance Perovskite-Sensitized Solar Cells. *Nature* **2013**, *499*, 316–319.

6. Yakunin, S.; Sytnyk, M.; Kriegner, D.; Shrestha, S.; Richter, M.; Matt, G. J.; Azimi, H.; Brabec, C. J.; Stangl, J.; Kovalenko, M. V. et al. Detection of X-Ray Photons by Solution-Processed Lead Halide Perovskites. *Nat. Photonics* **2015**, *9*, 444–449.

7. Dou, L. T.; Yang, Y.; You, J. B.; Hong, Z. R.; Chang, W. H.; Li, G. Solution-Processed Hybrid Perovskite Photodetectors with High Detectivity. *Nat. Commun.* **2014**, *5*.

8. Tan, Z. K.; Moghaddam, R. S.; Lai, M. L.; Docampo, P.; Higler, R.; Deschler, F.; Price, M.; Sadhanala, A.; Pazos, L. M.; Credgington, D. et al. Bright Light-Emitting Diodes Based on Organometal Halide Perovskite. *Nat. Nanotechnol.* **2014**, *9*, 687–692.

9. Xing, G. C.; Mathews, N.; Lim, S. S.; Yantara, N.; Liu, X. F.; Sabba, D.; Gratzel, M.; Mhaisalkar, S.; Sum, T. C. Low-Temperature Solution-Processed Wavelength-Tunable Perovskites for Lasing. *Nat. Mater.* **2014**, *13*, 476–480.

10. Yakunin, S.; Protesescu, L.; Krieg, F.; Bodnarchuk, M. I.; Nedelcu, G.; Humer, M.; De Luca, G.; Fiebig, M.; Heiss, W.; Kovalenko, M. V. Low-threshold amplified spontaneous emission and lasing from colloidal nanocrystals of caesium lead halide perovskites. *Nat. Commun.* **2015**, *6*, 8056.

11. Zhang, F.; Zhong, H.; Chen, C.; Wu, X.-g.; Hu, X.; Huang, H.; Han, J.; Zou, B.; Dong, Y. Brightly Luminescent and Color-Tunable Colloidal CH3NH3PbX3 (X = Br, I, Cl) Quantum Dots: Potential Alternatives for Display Technology. *ACS Nano* **2015**, *9*, 4533–4542.

12. Zhu, F.; Men, L.; Guo, Y.; Zhu, Q.; Bhattacharjee, U.; Goodwin, P. M.; Petrich, J. W.; Smith, E. A.; Vela, J. Shape Evolution and Single Particle Luminescence of Organometal Halide Perovskite Nanocrystals. *ACS Nano* **2015**, *9*, 2948–2959.

13. Schmidt, L. C.; Pertegás, A.; González-Carrero, S.; Malinkiewicz, O.; Agouram, S.; Mínguez Espallargas, G.; Bolink, H. J.; Galian, R. E.; Pérez-Prieto, J. Nontemplate Synthesis of CH3NH3PbBr3 Perovskite Nanoparticles. *J. Am. Chem. Soc.* **2014**, *136*, 850–853.

14. Tyagi, P.; Arveson, S. M.; Tisdale, W. A. Colloidal Organohalide Perovskite Nanoplatelets Exhibiting Quantum Confinement. *J. Phys. Chem. Lett.* **2015**, *6*, 1911–1916.

15. Jang, D. M.; Park, K.; Kim, D. H.; Park, J.; Shojaei, F.; Kang, H. S.; Ahn, J. P.; Lee, J. W.; Song, J. K. Reversible Halide Exchange Reaction of Organometal Trihalide Perovskite Colloidal Nanocrystals for Full-Range Band Gap Tuning. *Nano Lett.* **2015**, *15*, 5191–5199.

16. Horvath, E.; Spina, M.; Szekrenyes, Z.; Kamaras, K.; Gaal, R.; Gachet, D.; Forro, L. Nanowires of Methylammonium Lead Iodide CH3NH3Pbl3 Prepared by Low Temperature Solution-Mediated Crystallization. *Nano Lett.* **2014**, *14*, 6761–6766.

17. Ayguler, M. F.; Weber, M. D.; Puscher, B. M. D.; Medina, D. D.; Docampo, P.; Costa, R. D. Light-Emitting Electrochemical Cells Based on Hybrid Lead Halide Perovskite Nanoparticles. *J. Phys. Chem. C* **2015**, *119*, 12047–12054.

18. Protesescu, L.; Yakunin, S.; Bodnarchuk, M. I.; Krieg, F.; Caputo, R.; Hendon, C. H.; Yang, R. X.; Walsh, A.; Kovalenko, M. V. Nanocrystals of Cesium Lead Halide Perovskites (CsPbX3, X = Cl, Br, and I): Novel Optoelectronic Materials Showing Bright Emission with Wide Color Gamut. *Nano Lett.* **2015**, *15*, 3692–3696.

19. Nedelcu, G.; Protesescu, L.; Yakunin, S.; Bodnarchuk, M. I.; Grotevent, M. J.; Kovalenko, M. V. Fast Anion-Exchange in Highly Luminescent Nanocrystals of Cesium Lead Halide Perovskites (CsPbX3, X = Cl, Br, I). *Nano Lett.* **2015**, *15*, 5635Ű5640.

20. Zhang, D.; Eaton, S. W.; Yu, Y.; Dou, L.; Yang, P. Solution-Phase Synthesis of Cesium Lead Halide Perovskite Nanowires. *J. Am. Chem. Soc.* **2015**, *137*, 9230–9233.

21. Akkerman, Q. A.; D'Innocenzo, V.; Accornero, S.; Scarpellini, A.; Petrozza, A.; Prato, M.; Manna, L. Tuning the Optical Properties of Cesium Lead Halide Perovskite Nanocrystals by Anion Exchange Reactions. *J. Am. Chem. Soc.* **2015**, *137*, 10276–10281.

22. Green, M. L. H. A New Approach to the Formal Classification of Covalent Compounds of the Elements. *J. Organomet. Chem.* **1995**, *500*, 127–148.

23. Green, M. L. H.; Parkin, G. Application of the Covalent Bond Classification Method for the Teaching of Inorganic Chemistry. *J. Chem. Educ.* **2014**, *91*, 807–816.

24. Fritzinger, B.; Capek, R. K.; Lambert, K.; Martins, J. C.; Hens, Z. Utilizing Self-Exchange To Address the Binding of Carboxylic Acid Ligands to CdSe Quantum Dots. *J. Am. Chem. Soc.* **2010**, *132*, 10195–10201.

25. De Roo, J.; Justo, Y.; De Keukeleere, K.; Van den Broeck, F.; Martins, J. C.; Van Driessche, I.; Hens, Z. Carboxylic-Acid-Passivated Metal Oxide Nanocrystals: Ligand Exchange Characteristics of a New Binding Motif. *Angew. Chem. Int. Edit.* **2015**, *54*, 6488–6491.

26. De Roo, J.; Van den Broeck, F.; De Keukeleere, K.; Martins, J. C.; Van Driessche, I.; Hens, Z. Unravelling the Surface Chemistry of Metal Oxide Nanocrystals, the Role of Acids and Bases. *J. Am. Chem. Soc.* **2014**, *136*, 9650–9657.

27. Anderson, N. C.; Hendricks, M. P.; Choi, J. J.; Owen, J. S. Ligand Exchange and the Stoichiometry of Metal Chalcogenide Nanocrystals: Spectroscopic Observation of Facile Metal-Carboxylate Displacement and Binding. *J. Am. Chem. Soc.* **2013**, *135*, 18536–18548.

28. Cros-Gagneux, A.; Delpech, F.; Nayral, C.; Cornejo, A.; Coppel, Y.; Chaudret, B. Surface Chemistry of InP Quantum Dots: A Comprehensive Study. *J. Am. Chem. Soc.* **2010**, *132*, 18147–18157.

29. Valdez, C. N.; Schimpf, A. M.; Gamelin, D. R.; Mayer, J. M. Low Capping Group Surface Density on Zinc Oxide Nanocrystals. *ACS Nano* **2014**, *8*, 9463–9470.

30. Protesescu, L.; Nachtegaal, M.; Voznyy, O.; Borovinskaya, O.; Rossini, A. J.; Emsley, L.; Copéret, C.; Gunther, D.; Sargent, E. H.; Kovalenko, M. V. Atomistic Description of Thiostannate-Capped CdSe Nanocrystals: Retention of Four-Coordinate SnS4 Motif and Preservation of Cd-Rich Stoichiometry. *J. Am. Chem. Soc.* **2015**, *137*, 1862–1874.

31. Morris-Cohen, A. J.; Frederick, M. T.; Lilly, G. D.; McArthur, E. A.; Weiss, E. A. Organic Surfactant-Controlled Composition of the Surfaces of CdSe Quantum Dots. *J. Phys. Chem. Lett.* **2010**, *1*, 1078–1081.

32. Moreels, I.; Fritzinger, B.; Martins, J. C.; Hens, Z. Surface Chemistry of Colloidal PbSe Nanocrystals. *J. Am. Chem. Soc.* **2008**, *130*, 15081–15086.

33. Morris-Cohen, A. J.; Donakowski, M. D.; Knowles, K. E.; Weiss, E. A. The Effect of a Common Purification Procedure on the Chemical Composition of the Surfaces of CdSe Quantum Dots Synthesized with Trioctylphosphine Oxide. *J. Phys. Chem. C* **2010**, *114*, 897–906.

34. Hassinen, A.; Moreels, I.; De Nolf, K.; Smet, P. F.; Martins, J. C.; Hens, Z. Short-Chain Alcohols Strip X-Type Ligands and Quench the Luminescence of PbSe and CdSe Quantum Dots, Acetonitrile Does Not. *J. Am. Chem. Soc.* **2012**, *134*, 20705–20712.

35. Fritzinger, B.; Moreels, I.; Lommens, P.; Koole, R.; Hens, Z.; Martins, J. C. In Situ Observation of Rapid Ligand Exchange in Colloidal Nanocrystal Suspensions Using Transfer NOE Nuclear Magnetic Resonance Spectroscopy. *J. Am. Chem. Soc.* **2009**, *131*, 3024–3032.

36. Hens, Z.; Moreels, I. Light Absorption by Colloidal Semiconductor Quantum Dots. *J. Mater. Chem.* **2012**, *22*, 10406–10415.

37. Murtaza, G.; Ahmad, I. First Principle Study of the Structural and Optoelectronic Properties of Cubic Perovskites CsPbM3 (M=Cl, Br, I). *Physica B* **2011**, *406*, 3222–3229.

38. Hens, Z.; Martins, J. C. A Solution NMR Toolbox for Characterizing the Surface Chemistry of Colloidal Nanocrystals. *Chem. Mater.* **2013**, *25*, 1211–1221.

39. Van Lokeren, L.; Maheut, G.; Ribot, F.; Escax, V.; Verbruggen, I.; Sanchez, C.; Martins, J. C.; Biesemans, M.; Willem, R. Characterization of Titanium Dioxide Nanoparticles Dispersed in Organic Ligand Solutions by Using a Diffusion-Ordered Spectroscopy-Based Strategy. *Chem. Eur. J.* **2007**, *13*, 6957–6966.

40. Sangeetha, N. M.; Gauvin, M.; Decorde, N.; Delpech, F.; Fazzini, P. F.; Viallet, B.; Viau, G.; Grisolia, J.; Ressier, L. A Transparent Flexible Z-Axis Sensitive Multi-Touch Panel Based on Colloidal ITO Nanocrystals. *Nanoscale* **2015**, *7*, 12631–12640.

41. Matioszek, D.; Ojo, W. S.; Cornejo, A.; Katir, N.; El Ezzi, M.; Le Troedec, M.; Martinez, H.; Gornitzka, H.; Castel, A.; Nayral, C. et al. From Rational Design of Organometallic Precursors to Optimized Synthesis of Core/Shell Ge/GeO2 Nanoparticles. *Dalton Trans.* **2015**, *44*, 7242–7250.

42. Dierick, R.; Van den Broeck, F.; De Nolf, K.; Zhao, Q.; Vantomme, A.; Martins, J. C.; Hens, Z. Surface Chemistry of CuInS2 Colloidal Nanocrystals, Tight Binding of L-Type Ligands. *Chem. Mater.* **2014**, *26*, 5950–5957.

43. Van Lokeren, L.; Willem, R.; van der Beek, D.; Davidson, P.; Morris, G. A.; Ribot, F. Probing the Anions Mediated Associative Behavior of Tin-12 Oxo-Macrocations by Pulsed Field Gradient NMR Spectroscopy. *J. Phys. Chem. C* **2010**, *114*, 16087–16091.

44. Hubbard, J. B.; Douglas, J. F. Hydrodynamic Friction of Arbitrarily Shaped Brownian Particles. *Phys. Rev. E* **1993**, *47*, R2983–R2986.

45. Douglas, J. F.; Zhou, H. X.; Hubbard, J. B. Hydrodynamic Friction and the Capacitance of Arbitrarily Shaped Objects. *Phys. Rev. E* **1994**, *49*, 5319–5337.

46. Gomes, R.; Hassinen, A.; Szczygiel, A.; Zhao, Q. A.; Vantomme, A.; Martins, J. C.; Hens, Z. Binding of Phosphonic Acids to CdSe Quantum Dots: A Solution NMR Study. *J. Phys. Chem. Lett.* **2011**, *2*, 145–152.

47. Owen, J. S.; Park, J.; Trudeau, P. E.; Alivisatos, A. P. Reaction chemistry and ligand exchange at cadmium-selenide nanocrystal surfaces. *J. Am. Chem. Soc.* **2008**, *130*, 12279–12280.

48. Connell, M. A.; Bowyer, P. J.; Bone, P. A.; Davis, A. L.; Swanson, A. G.; Nilsson, M.; Morris, G. A. Improving the Accuracy of Pulsed Field Gradient NMR Diffusion Experiments: Correction for Gradient Non-Uniformity. *J. Magn. Reson.* **2009**, *198*, 121–131.

49. Sinnaeve, D. The Stejskal-Tanner Equation Generalized for any Gradient Shape-an Overview of Most Pulse Sequences Measuring Free Diffusion. *Concepts Magn. Reson.* **2012**, *40A*, 39–65.

Graphical TOC Entry